

Article

Influence of Soil Colloids on the Transport of Cd²⁺ and Pb²⁺ under Different pH and Ionic Strength Conditions

Zihao Ye ¹, Dihao Xu ¹, Jiawen Zhong ¹, Shuang Gao ¹, Jinjin Wang ^{1,2,3} , Yulong Zhang ^{1,2,3}, Huijuan Xu ^{1,2,3}, Yongtao Li ^{1,2,3} and Wenyan Li ^{1,2,3,*} 

- ¹ College of Natural Resources and Environment, Joint Institute for Environmental Research & Education, South China Agricultural University, Guangzhou 510642, China; yzh@stu.scau.edu.cn (Z.Y.); 00806@stu.scau.edu.cn (D.X.); zhongjiawen@stu.scau.edu.cn (J.Z.); yxtabmax@outlook.com (S.G.); wangjinjin@scau.edu.cn (J.W.); yulongzhang@scau.edu.cn (Y.Z.); hjxu@scau.edu.cn (H.X.); yongtao@scau.edu.cn (Y.L.)
- ² Key Laboratory of Arable Land Conservation (South China), MOA, South China Agricultural University, Guangzhou 510642, China
- ³ Guangdong Province Key Laboratory for Land Use and Consolidation, South China Agricultural University, Guangzhou 510642, China
- * Correspondence: lily1984191@scau.edu.cn

Abstract: The co-transport of contaminants by soil colloids can generate substantial environmental risk, and this behavior is greatly affected by environmental conditions. In this study, AF4-ICP-MS was used to investigate the size distribution and composition of Cd/Pb-bearing colloids; saturated sand column experiments were used to investigate the impact of soil colloids on the transport of Cd/Pb under different pH and ionic strength conditions. AF4-ICP-MS characterization showed that natural colloids were primarily associated with two sizes ranges: 0.3–35 KDa (F1, fine nanoparticles) and 280 KDa–450 nm (F2, larger nanoparticles), which mainly consisted of organic matter (OM), iron (Fe), and manganese (Mn) (oxy)hydroxides and clay minerals. Fine nanoparticles could strongly adsorb Cd and Pb under all environmental conditions. Mn and Fe (oxy)hydroxides generally formed under neutral to alkaline conditions and exhibited adsorption capabilities for Cd and Pb, respectively. Transport experiments were conducted under different pH and ionic strength conditions. At pH 3.0, soil colloids had little effect on the transport of Cd²⁺ and Pb²⁺. At pH 5.0, soil colloids inhibited the transport of Cd²⁺ by 16.1%, and Pb²⁺ recovery was still 0.0%. At pH 7.0 and 9.0, soil colloids facilitated the transport of Cd²⁺ by 15.6% and 29.6%, facilitated Pb²⁺ by 1.3% and 6.4%. At an ionic strength of 0, 0.005, and 0.01 mol L⁻¹ NaNO₃, soil colloids facilitated the transport of Cd²⁺ by 77.7%, 45.8%, and 15.6%, only facilitated the transport of Pb²⁺ by 46.2% at an ionic strength of 0 mol L⁻¹ NaNO₃. At an ionic strength of 0.05 mol L⁻¹ NaNO₃, soil colloids inhibited the transport of Cd²⁺ and Pb²⁺ by 33.1% and 21.0%, respectively. The transport of Cd²⁺ and Pb²⁺ facilitated by soil colloids was clearly observed under low ionic strength and non-acidic conditions, which can generate a potential environmental risk.

Keywords: Cd; Pb; soil colloids; field-flow fractionation; nanoparticles; transport



Citation: Ye, Z.; Xu, D.; Zhong, J.; Gao, S.; Wang, J.; Zhang, Y.; Xu, H.; Li, Y.; Li, W. Influence of Soil Colloids on the Transport of Cd²⁺ and Pb²⁺ under Different pH and Ionic Strength Conditions. *Agronomy* **2024**, *14*, 352. <https://doi.org/10.3390/agronomy14020352>

Academic Editor: David Houben

Received: 27 December 2023

Revised: 2 February 2024

Accepted: 3 February 2024

Published: 9 February 2024



Copyright: © 2024 by the authors. Licensee MDPI, Basel, Switzerland. This article is an open access article distributed under the terms and conditions of the Creative Commons Attribution (CC BY) license (<https://creativecommons.org/licenses/by/4.0/>).

1. Introduction

Heavy metals have been introduced to soil by human activities, such as the burning of fossil fuels, industrial effluents, mining, and smelting activities [1–3]. Most heavy metals are stabilized by adsorption, complexation, and precipitation after being discharged into the soil [1,4,5]. Soil colloids are the most active constituent in the soil due to their small sizes, large surface areas, and high surface charges [1,4,5]. Many researchers have shown that colloids in soil are able to transport through preferential flow, macropores, or cracks [4,6,7]. Soil colloids, such as clay minerals, soil organic matter (OM), and iron (Fe)/aluminum (Al) (oxy)hydroxide, generally possess a high adsorption capacity for heavy metals [8,9],

which means the movement of soil colloids has become an important mechanism for the transport of heavy metals in soil [10,11]. The colloidal transport of heavy metals has been observed by many researchers [12–14], and it is significantly influenced by environmental conditions [15,16]. For example, freeze–thaw cycles in soils change the dispersibility of colloids and affect the transport of lead (Pb) [17]. Upon the lowering of initial soil moisture, the increased transport of colloids but decreased transport of colloid-associated cadmium (Cd) was observed [18]. Under alkaline conditions of pH 7.8, soil colloids significantly facilitate the transport of arsenic (As) and chromium (Cr), but to a lesser extent facilitate the transport of cuprum (Cu) and cadmium (Cd) [19]. Redox fluctuation results in the dissolution of Fe/Mn-(oxy)hydroxide and sulfide phases and heavy metal release to soil porewater [20]. The colloidal transport of heavy metals in soil is complex, and most conclusions are based on laboratory research, lacking studies under natural conditions.

The recent emergence of asymmetric flow field-flow fractionation (AF4) coupled with online detection systems allows for the quantification and continuous size fractionation of natural colloids in soil extracts [21] and is capable of detecting soil colloids down to the low nanometer, which are of particular environmental importance [22–24]. In addition, a water-saturated sand column experiment is usually used to investigate the transport behaviors of heavy metals. Hydrus-1D (4.17.0140) is a software for simulating the one-dimensional movement of multiple solutes [25]. It can analyze the data of column experiments by using mathematical models to obtain parameters that can be used to describe the transport behavior of heavy metals and soil colloids [25,26].

Cd and Pb are commonly found in sites contaminated by heavy metals [27]. The transport of Cd and Pb in subsurface can cause serious groundwater pollution, and poses a severe threat to human health. To obtain a better understanding of the fate and transport of Cd and Pb corresponding to soil colloids, the present study applied the AF4-UV-ICP-MS technology and Hydrus-1D mathematical model to describe Cd and Pb that interacts with soil colloids under different pH and ionic strength conditions (IS). The objectives of this study are as follows: (a) to investigate the size distribution and composition of Cd/Pb-bearing colloids in contaminated soil under different natural conditions from three contaminated sites, (b) to investigate the transport behavior of Cd and Pb with soil colloids under different pH and ionic strength conditions, which could contribute to understanding the colloidal transport of Cd and Pb in the subsurface.

2. Materials and Methods

2.1. Soil Colloids Preparation and Analysis

Soil samples were collected from the surface (0–20 cm) of three contaminated sites in proximity to mining and smelting operations. Dabao Mountain (DBS, pH = 5.5) soil was originally a paddy field and was abandoned for years due to contamination. It was contaminated by atmospheric deposition and irrigation water polluted by polymetallic deposit (Cu, Fe, Zn, etc.) mining activities from the Polymetallic Mining Area in Shao guan City, Guangdong Province. Hulu Dao (HD, pH = 7.0) soil was natural soil used for agriculture years ago and was contaminated by atmospheric deposition and irrigation water polluted by sewage from a Zinc Smelter in Hulu Dao City, Liaoning Province. Shen yang (SY, pH = 8.0) soil was natural soil contaminated by atmospheric deposition due to the emitted dusts from a multi-metal smelter in Shenyang City, Liaoning Province. The basic chemical parameters for three contaminated soils are shown in Table S1. According to Stokes' law, soil colloids (<1 μm) were collected by sedimentation siphoning.

Particle size distributions and the zeta potential of soil colloids were analyzed using a Laser Particle Size Analyzer (Zetasizer Nano ZS 90, Malvern, England;), the particle sizes of soil colloids were as follows: DBS = 170 ± 3 nm, HD = 158 ± 6 nm, SY = 141 ± 3 nm. Soil colloids were scanned at full UV wavelengths (UV-2600, Shimadzu, Tokyo, Japan; –5–5 Abs, 185–900 nm; Figure S1), and the final wavelength of 254 nm was chosen for the experiments. The concentration of soil colloids in the collecting solution was analyzed by UV spectrophotometer (254 nm). Soil colloid concentration is proportional to absorbance

(Figure S2). After the addition of HNO₃ (sample/HNO₃ = 10:1, *v/v*) to the collecting solution, the concentrations of Cd and Pb were measured by ICP-OES (Agilent 5100, Agilent, Palo Alto, CA, USA; RF power 1.2 kW; nebulizer flow 0.95 L min⁻¹, pumping rate 1.0 mL min⁻¹). The emission lines were selected for Cd (228.8 nm), Pb (220.4 nm), Fe (259.9 nm), Mn (257.6 nm), Al (308.2 nm) and measured ¹¹¹Cd, ²⁰⁸Pb, ⁵⁵Mn, ⁵⁶Fe, ²⁷Al.

2.2. Asymmetric Flow Field-Flow Fractionation

Soil colloids solution (450 nm filtered) is characterized by AF4 (AF 2000, Postnova Analytics, Landsberg, Germany; injection volumes were 850 µL) coupled with a UV–vis detector (UV, SPD-20A, Landsberg, Germany; absorption wavelength selected at 254 nm) and ICP-MS (Agilent 8800, Agilent, Palo Alto, CA, USA). A 0.3 kDa nominal cut-off polyether sulfone membrane was used as the accumulation wall. The carrier solution flowing in the AF4 was 5 mM NaCl (100 nm filtered, pH = 7.0). A focusing time of 5 min and a crossflow rate of 3.5 mL min⁻¹ were used to optimize the size fractionation of colloids or the total recovery. The elution runs ended with a washing step after 40 min with the crossflow rate linearly decreasing to 0 mL/min within 15 min, allowing the elution of the remaining non-fractionated particles. To translate the retention time into molecular weight, we used a combination of external calibrations with polystyrene sulfonate standards (nominal molecular weights of 1.4–280 kDa, Figure S3).

2.3. Column Experiment

A certain volume of stock solution of Cd²⁺ and Pb²⁺ was added to a predetermined volume of soil particle suspensions to prepare influent suspensions, after which the mixed suspensions were diluted with NaNO₃ solution. Final concentrations of soil colloids and Cd²⁺ and Pb²⁺ in the influent suspensions were 100 and 10 mg L⁻¹, respectively. The transport experiments were carried out under different pH solutions (3.0, 5.0, 7.0, and 9.0) and IS (0, 0.005, 0.01, and 0.05 mol L⁻¹ NaNO₃). The mixed solutions of soil colloids and Cd²⁺ and Pb²⁺ were equilibrated for 12 h before co-transport experiments, and stirred constantly during the transport experiments.

The quartz sand (Aladdin Company, Shanghai, China; 0.105–0.71 mm) was sieved to 0.25–0.3 mm and washed with deionized water until it was clear. The sand was soaked in 10% HNO₃ for 48 h, then washed with deionized water to a neutral state and soaked in 1 mol L⁻¹ NaOH for 48 h, and finally washed with deionized water to a neutral state and dried at 60 °C. The transport apparatus for soil colloids is shown in Figure S4. The columns were 3 cm in diameter and 14 cm in height, and were filled with quartz sand using the wet packing method. The pores were evenly distributed and free of air bubbles.

Deionized water was introduced upward to the column with a peristaltic pump for 24 h to make the current velocity (*q*, 1 mL min⁻¹) steady. A 5 pore volume (PV) KBr solution (1 mol L⁻¹) was pumped into the sand column to obtain the breakthrough curve (BTC) of Br⁻, which was fitted by an advection–dispersion equation by Hydrus-1D to obtain the dispersion coefficient (*D*).

A 5 PV background solution (*q*, 1 mL min⁻¹) was pumped upward in the column, then 5 PV experimental solutions were pumped in the column, and a 10 PV background solution was pumped in the column to finally flush it. The effluent was collected in regular time (10 min) intervals using a fraction collector.

2.4. Hydrus-1D Model

The breakthrough curves of soil colloids and heavy metal ions in saturated porous media were simulated using a two-dynamic convection–dispersion model, which can be described by the following equations:

$$\frac{\partial \theta C}{\partial t} + \rho \frac{\partial S}{\partial t} = \frac{\partial}{\partial z} \left(\theta D \frac{\partial C}{\partial z} \right) - \frac{\partial q C}{\partial z} \quad (1)$$

$$\rho \frac{\partial S}{\partial t} = \theta k_a \left(1 - \frac{S}{S_{\max}}\right) C - k_d \rho S \quad (2)$$

where C is the concentration of soil colloids or heavy metals ions (mg L^{-1}), t is the time (min), v is the velocity ($\text{cm} \cdot \text{min}^{-1}$), D is the dispersion coefficient ($\text{cm}^2 \cdot \text{min}^{-1}$), ρ is the media bulk density ($\text{g} \cdot \text{cm}^{-3}$), θ is the porosity, z is the transport distance (cm), k_a is the attachment coefficient (min^{-1}), k_d is the detachment coefficient (min^{-1}), and S_{\max} is the maximum solid phase concentration ($\text{mg} \cdot \text{g}^{-1}$). The breakthrough curves of soil colloids and Cd and Pb were simulated and inversely fitted using Hydrus-1D.

3. Results and Discussion

3.1. AF4 and Elemental Analysis of Different Soil Colloids

The AF4 fractograms of natural soil colloid solutions from three contaminated sites are shown in Figure 1. UV_{254} has been validated as a good proxy for OM colloids [28]. Based on the AF4 fractograms, two main fractions of soil colloids were identified. The first colloidal fraction (F1) was distinct with a retention time between 0 and 10 min and corresponded to a fraction with a particle size of 0.3–35 kDa, and here defined as fine nanoparticles. In this fraction, the co-elution of abundant OM, Fe, Al, and Mn was detected, which meant that all elements were highly enriched in fine nanoparticles. The fine nanoparticles which were ubiquitous in all soil colloid solutions were composed of OM, Fe, and Mn (oxy)hydroxides and clay minerals [29]. The consistency of the signal peaks might imply the close relation between Fe, Mn, OM, and clay, similar to that of Fe-OM-clay colloids found in another study [30]. The second fraction (F2) was identified after 35 min and corresponded to the remaining non-fractionated particles that were larger than 280 kDa but smaller than 450 nm (solutions were 450 nm filtered), and here defined as larger nanoparticles. In this fraction, the signal peaks of OM, Fe, Al, and Mn were found to be neglectable in acidic DBS soil solution; this corresponded with the research by Hu [20], which suggested that acidic conditions would inhibit the formation of colloids in F2. The signal peaks of Fe and Al simultaneously emerged at the same time in HD and SY solutions, indicating a high correlation between Fe and Al. Fe and Al were likely to form Fe–clay complexes of similar particle sizes. OM also exhibited some degree of correlation with both Fe and Al, but its signal peak emerged marginally ahead of the peaks for Fe and Al in HD and lagged slightly in SY. The signal peak of Mn was significantly observed in the SY alkaline solution, and emerged marginally ahead of the peaks for Fe and Al. In summary, soil solutions from three contaminated sites mainly contained fine nanoparticles and larger nanoparticles which were distributed in F1 and F2 fractions, respectively. The nanoparticles were composed of a complex assemblage of multiple elements and clay minerals, exhibiting high stability and mobility. The formation of larger nanoparticles was primarily influenced by the pH of the solution, and the alkaline condition was more favorable for forming Fe–clay colloids and Mn (oxy)hydroxides. OM was also highly correlated with Fe and Al, and previous studies had suggested that OM could confer electrostatic and steric stability to Fe (oxy)hydroxide colloids and Fe (oxy)hydroxide–clay complexes [31], thereby enhancing the dispersibility and mobility of the colloids.

The signals of Cd showed significant instability; the same phenomenon could be observed in another study [22], which meant the high activity of Cd. But in F1, Cd showed a significant signal peak and was consistent with that of other elements, indicating the strong and stable adsorption ability of fine nanoparticles. Cd-bearing fine nanoparticles were ubiquitous in all soil solutions under different pH conditions. In F1 (10 min), Cd showed another special peak in HD soil solution, and Mn also showed a weak peak at the same time. The fractograms of Cd and Mn demonstrated a notable similarity in F1 and F2 for all soil solutions, which implied that Cd might be coupled to Mn colloids in soil solution. In F2, the transport of Cd carried by larger nanoparticles was comparatively low and was likely to be affected by the pH of the solution. In the SY soil solution, the alkaline condition facilitated the formation of Mn and Fe (oxy)hydroxide. The fractograms of Cd, Mn, and Fe showed similarity. Cd could be fixed on the surface OH group of Mn

and Fe colloids by ion exchange [32]. Mn and Fe were likely to be the primary carrier for Cd, which could enhance the transport of Cd.

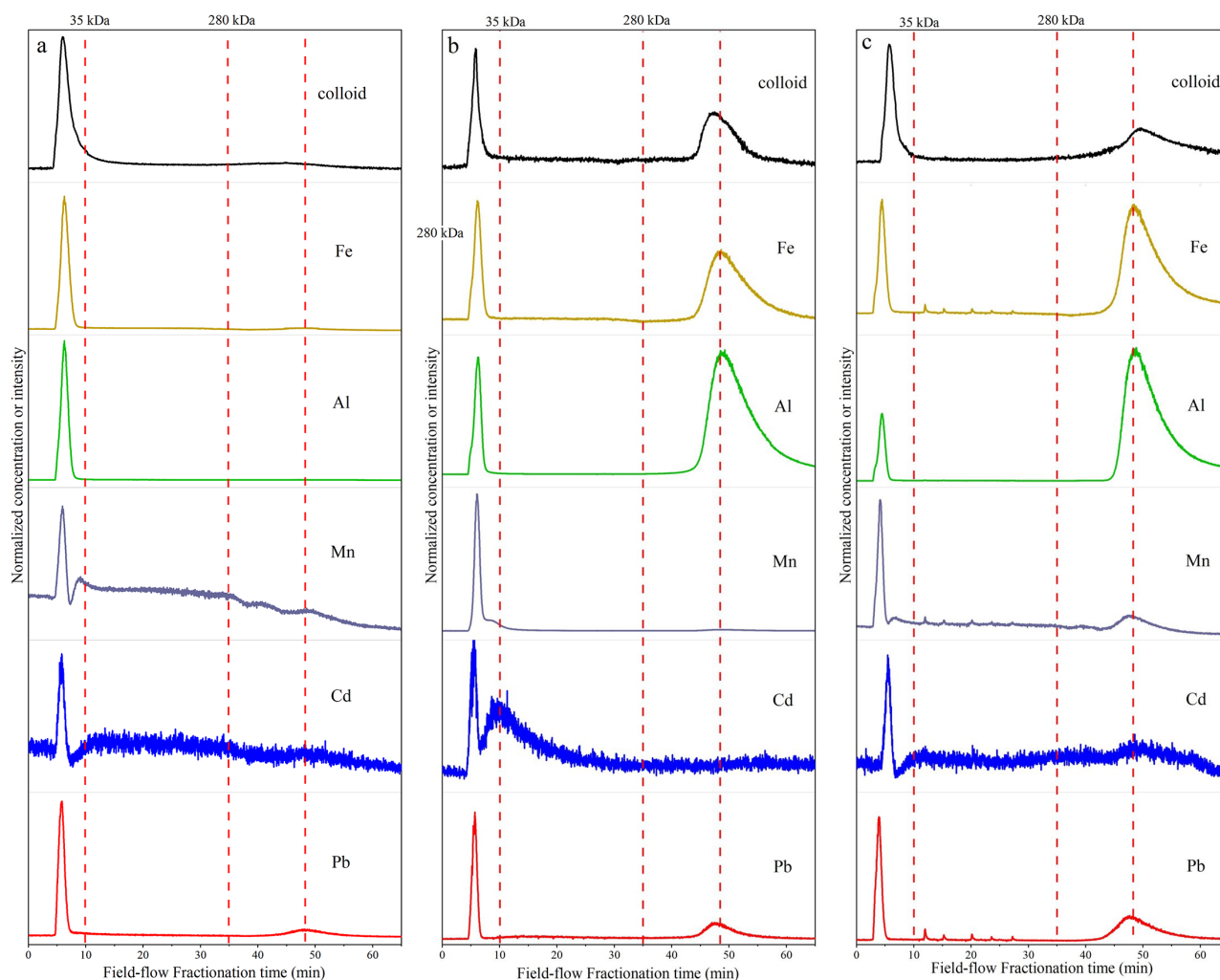


Figure 1. AF4 fractograms of three different soil colloids: (a) DBS soil colloid, pH = 5.5; (b) HD soil colloid, pH = 7.0; and (c) SY soil colloid, pH = 8.0.

The signal peaks of Pb were significantly observed in both F1 and F2, indicating that the Pb-bearing fine and larger nanoparticles existed in all soil solutions. Pb also showed a high correlation with OM, Fe, and Al, and its fractograms were highly similar to the fractograms of Fe. There were several small signal peaks of Fe and Mn emerging within the fraction range from 35 to 280 kDa, indicating the formation of Fe and Mn (oxy)hydroxide for different particle sizes in the alkaline SY soil solution. Noting that the signal peaks of Pb detected simultaneously emerged with signal peaks of Fe and Mn in this fraction, indicating a strong adsorption of Pb by Fe/Mn (oxy)hydroxide. Pb could also be fixed on the surface OH group of Fe/Mn colloids like Cd. Pb could be more stably bound to colloid than Cd; this was also observed in another study [30]. Therefore, the transport of Pb was predominantly controlled by soil colloids, and environmental conditions that favored the formation of colloids, such as an increase in pH, would enhance the transport of Pb [17,19].

The AF4 characterization results demonstrated that fine nanoparticles and larger nanoparticles commonly existed in soil solutions. Fine nanoparticles were ubiquitous and relatively stable, exhibiting a strong adsorption capacity for Cd and Pb. This fraction was stable and less affected by environmental conditions [20,22], which means that it is an important component of Cd and Pb transport. Larger nanoparticles exhibited high stability in non-acidic solutions, and their adsorption of heavy metals is substantially influenced

by their composition. Cd transport could be influenced by Fe/Mn (oxy)hydroxide, and Pb was highly adsorbed by Fe/Mn (oxy)hydroxide. The formation and stability of Fe and Mn (oxy)hydroxide were sensitive to pH, the larger nanoparticles might be an important component of heavy metal transport in weakly acidic, neutral, and alkaline soils such as contaminated rice fields [20] and river flood plains [33]. Environmental conditions that affect the formation and stability of colloids can impact the transport of heavy metals, so we subsequently conducted a series of indoor saturated sand column transport experiments under different pH and ionic strength conditions.

3.2. Transport of Soil Colloids under Different pH and Ionic Strength Conditions

The BTC of Br⁻ tracer was symmetric and not retarded, and fitted well with the advection–dispersion equation ($R^2 = 0.9989$, Figure 2), indicating that the saturated sand column was free of the wall effect, a short circuit, and preferential flows. The fitted D value ($0.2518 \text{ cm}^2 \text{ h}^{-1}$) was used for the two-dynamic convection–dispersion model. All the soil colloid samples had good absorption at 254 nm. The concentration of soil colloid was found to have a strong linear correlation with the absorbance at 254 nm (Figure S2).

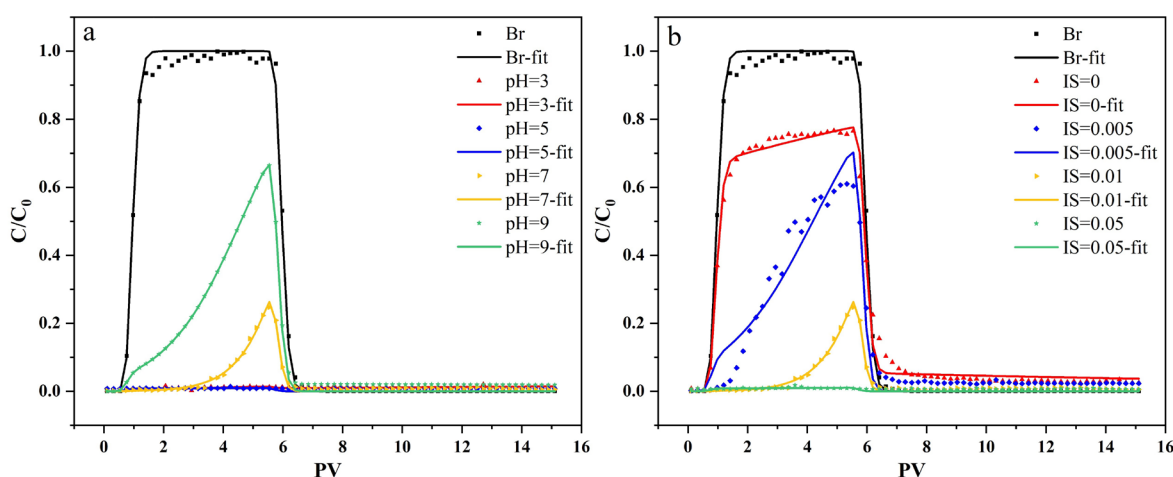


Figure 2. BTCs of soil colloids in the sand column under different pH (a) and ionic strength (b) conditions.

The BTCs of soil colloids under different pH and ionic strength conditions are shown in Figure 2; colloidal properties and fitting parameters are shown in Table 1. The BTCs fitted well with the two-dynamic model ($R^2 > 0.95$). Soil colloid recoveries at pH 3.0 and 5.0 with an ionic strength of $0.05 \text{ mol L}^{-1} \text{ NaNO}_3$ were too low for the model to be fitted. Soil colloid recoveries were 0.0%, 0.0%, 7.0%, and 32.5% at pH 3.0, 5.0, 7.0, and 9.0, respectively. The BTCs' peak of soil colloids at high pH was significantly higher than at low pH (Figure 2a); soil colloids were almost blocked in the column when pH fell to 5.0. Soil colloid recoveries were 81.6%, 39.2%, 7.0%, and 0.0% at IS 0, 0.005, 0.01, and $0.05 \text{ mol L}^{-1} \text{ NaNO}_3$, respectively. Soil colloids were blocked in the column when IS rose to $0.05 \text{ mol L}^{-1} \text{ NaNO}_3$ (Figure 2b). In conclusion, the acidic and high IS condition could inhibit the transport of soil colloids, including Cd/Pb-bearing colloids, but it does not mean that it is good for the environment. Acid rain acidifies soils and increases the IS, but activates heavy metal ions and promotes their transport [34].

At pH 9.0 and IS 0, soil colloids showed a higher peak and an initial breakthrough at lower PV, which indicate a stronger mobility. Sand grains and soil colloids were both negatively charged in all cases, indicating a repulsive force between them, the change in charge has a significant effect on the height of the BTCs peak as well as the time of initial breakthrough [35]. Decreasing pH and increasing ionic strength reduced the negative charges on the surface of soil colloids (Table 1), which reduced repulsive forces between soil colloids and sand grains, making soil colloids easier to aggregate and were blocked in

the column. The BTCs decreased sharply between 5–6 PV (flushing time) and the tailing of all BTCs were fairly weak. The phenomenon indicated that the deposit of soil colloids in the column was a physical retention mechanism, and the initial breakthrough for colloids was influenced by physical straining and filtration [10]. Remarkably, at high pH (9.0) and low IS (0), 67.5% and 18.7% of the soil colloids were blocked in the column. Although under unfavorable attachment conditions, the attachment between soil colloids and sand grains also occurs when attractive van der Waals interactions exceed repulsive electrostatic forces at short separation distances [36]. It may also be related to soil colloid type, sand particle size, and flow rate. The tension between the soil colloids and the porous medium increases as the ratio of the soil colloid diameter to the medium particle size increases, and the resistance generated by the low flow rate is not sufficient to disperse these colloids, leading to a blockage phenomenon [37]. In addition, Fe/Mn (oxy)hydroxides enhance the non-uniformity of the surface charge on soil colloids, which facilitates their attachment to sand grains [11].

Table 1. Soil colloid properties at different conditions and the fitting results.

Solution	pH	IS	Pore	Zeta (mV)	Particle (nm)	Recoveries	R ²
100 mg·L ⁻¹ soil colloids	3.0	0.01	0.46	-19.5 ± 0.2	1223 ± 29	NA ¹	
	5.0	0.01	0.46	-33.7 ± 0.3	468 ± 15	NA ¹	
	7.0	0.01	0.46	-34.6 ± 0.3	450 ± 11	7.0%	0.9943
	9.0	0.01	0.46	-35.9 ± 0.5	401 ± 10	32.5%	0.9820
	7.0	0	0.46	-36.2 ± 0.4	400 ± 10	81.6%	0.9950
	7.0	0.005	0.46	-35.8 ± 0.3	413 ± 12	39.2%	0.9657
	7.0	0.05	0.46	-25.2 ± 0.4	616 ± 19	NA ¹	

¹ NA: not applicable.

3.3. Transport of Cd²⁺ and Pb²⁺ under Different pH and Ionic Strength Conditions

The BTCs of Cd²⁺ and Pb²⁺ under different pH and ionic strength conditions are shown in Figure 3; fitting parameters are shown in Table 2. The BTCs fitted well with the two-dynamic model (R² > 0.90). The recoveries of Cd²⁺ and Pb²⁺ were 99.7% and 86.3%, 82.2% and 0.0%, 38.6% and 0.0%, and 0.0% and 0.0% at pH 3.0, 5.0, 7.0, and 9.0, respectively. The recoveries of Cd²⁺ and Pb²⁺ were 0.0% and 0.0%, 10.7% and 0.0%, 38.6% and 0.0%, and 47.7% and 21.0% at IS 0, 0.005, 0.01, and 0.05 mol L⁻¹ NaNO₃, respectively.

Table 2. The fitting results of Cd²⁺ and Pb²⁺ BTCs under different pH and ionic strength conditions.

Solution	pH	IS	Dispersion	Pore	Recoveries	R ²
10 mg·L ⁻¹ Cd ²⁺	3.0	0.01	0.2518	0.46	99.7%	0.9981
	5.0	0.01	0.2518	0.46	82.2%	0.9840
	7.0	0.01	0.2518	0.46	38.6%	0.9620
	9.0	0.01	0.2518	0.46	NA ¹	
	7.0	0	0.2518	0.46	NA ¹	
	7.0	0.005	0.2518	0.46	10.7%	0.9958
	7.0	0.05	0.2518	0.46	47.7%	0.9046
10 mg·L ⁻¹ Pb ²⁺	3.0	0.01	0.2518	0.46	86.3%	0.9926
	5.0	0.01	0.2518	0.46	NA ¹	
	7.0	0.01	0.2518	0.46	NA ¹	
	9.0	0.01	0.2518	0.46	NA ¹	
	5.0	0	0.2518	0.46	NA ¹	
	5.0	0.005	0.2518	0.46	NA ¹	
	5.0	0.05	0.2518	0.46	21.0%	0.9055

¹ NA: not applicable.

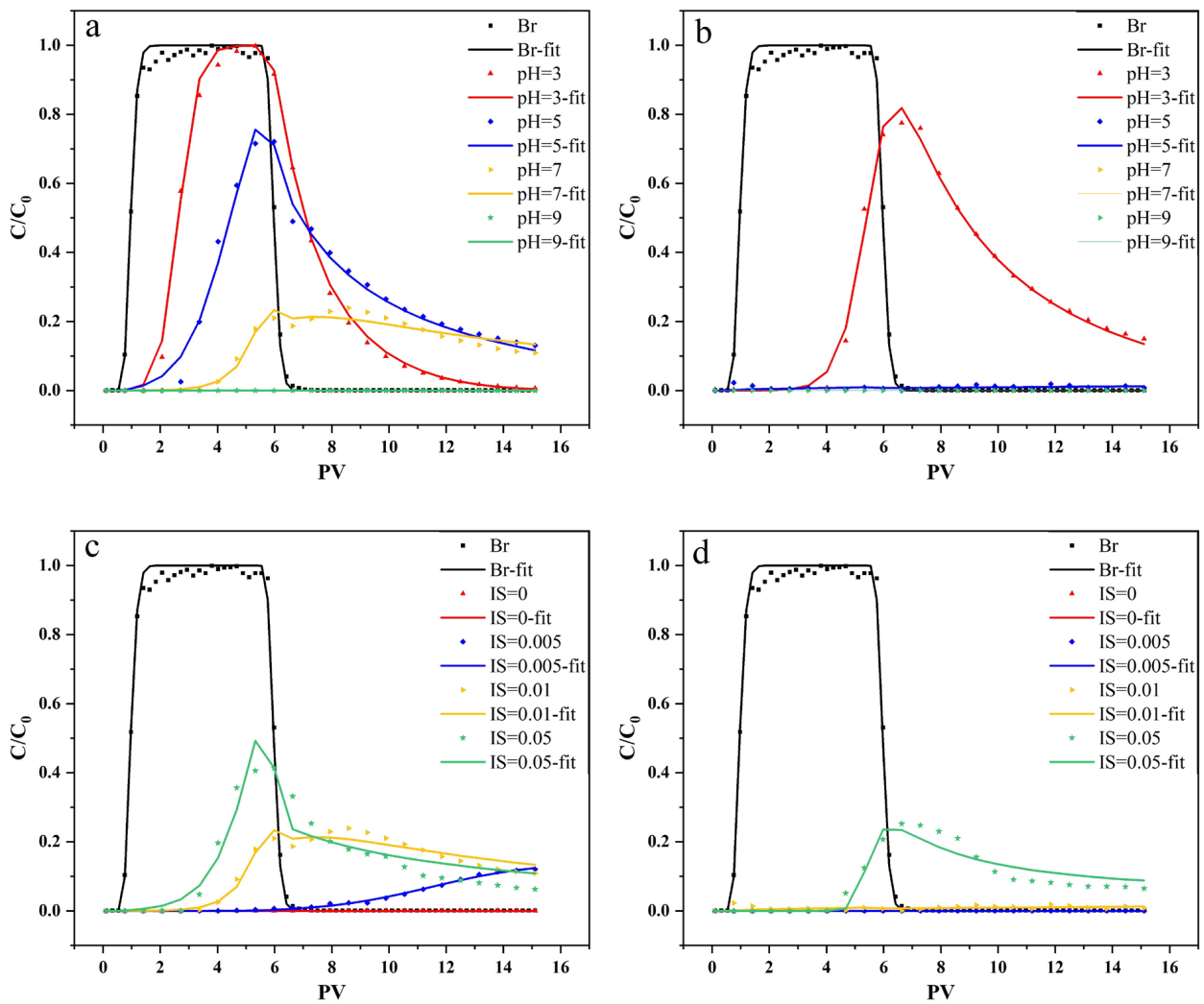


Figure 3. BTCs of Cd^{2+} (a,c) and Pb^{2+} (b,d) under different pH and ionic strength conditions.

The BTCs of Cd^{2+} and Pb^{2+} gradually decreased between 5–6 PV (flushing time) and showed a significant trailing phenomenon, indicating the existence of adsorption and desorption of the two ions by the sand grains (Figure 3); this has also occurred in prior studies [10,38]. The BTC tail results were different from soil colloids, indicating the different retention mechanism in the column between heavy metals and soil colloids. With increasing pH, the initial breakthrough appeared later and the BTCs' peak was lower, indicating the increasing adsorption capacity of sand grains. The Cd^{2+} and Pb^{2+} recoveries fell to 0.0% at a pH of 9.0 and 5.0 (Figure 3a,b). The phenomenon can be explained by the fact that the high-pH surface groups of the sand grains are strongly deprotonated ($\equiv\text{Si-OH} \leftrightarrow \equiv\text{Si-O}^- + \text{H}^+$), providing more negatively charged surface adsorption sites for the metal cation [25]. The Cd^{2+} recoveries increased significantly with increasing IS, indicating that higher ionic strength facilitated the desorption and transport of Cd^{2+} (Figure 3c). This could be interpreted as a competition for adsorption with background electrolyte cations at high IS [1]. Pb recoveries were 0.0% at an IS of 0, 0.005, and 0.01 mol L⁻¹ NaNO₃, and increased to 21.0% at IS 0.05 mol L⁻¹ NaNO₃, indicating the relatively weaker transport capacity.

3.4. Transport of Cd^{2+} and Pb^{2+} with Soil Colloids under Different pH and Ionic Strength Conditions

The BTCs of Cd^{2+} and Pb^{2+} transport with soil colloids under different pH and ionic strength conditions are shown in Figures 4 and 5; fitting parameters are shown in Table 3.

The recoveries of Cd^{2+} and Pb^{2+} were 99.6% and 81.4%, 66.2% and 0.0%, 54.3% and 12.4%, and 29.6% and 27.1% at pHs of 3.0, 5.0, 7.0, and 9.0, respectively. Cd^{2+} recoveries were larger than 0.0% at all pHs, and Pb^{2+} recoveries were 0.0% at pH of 5.0 only. The recoveries of Cd^{2+} and Pb^{2+} were 77.7% and 46.2%, 56.5% and 0.0%, 54.3% and 0.0%, and 14.6% and 0.0% at an IS of 0, 0.005, 0.01, and 0.05 mol L⁻¹ NaNO₃, respectively. Cd^{2+} recoveries were larger than Pb^{2+} at all pHs and ISs. These results mean that the transport ability of Cd^{2+} was much stronger than Pb^{2+} .

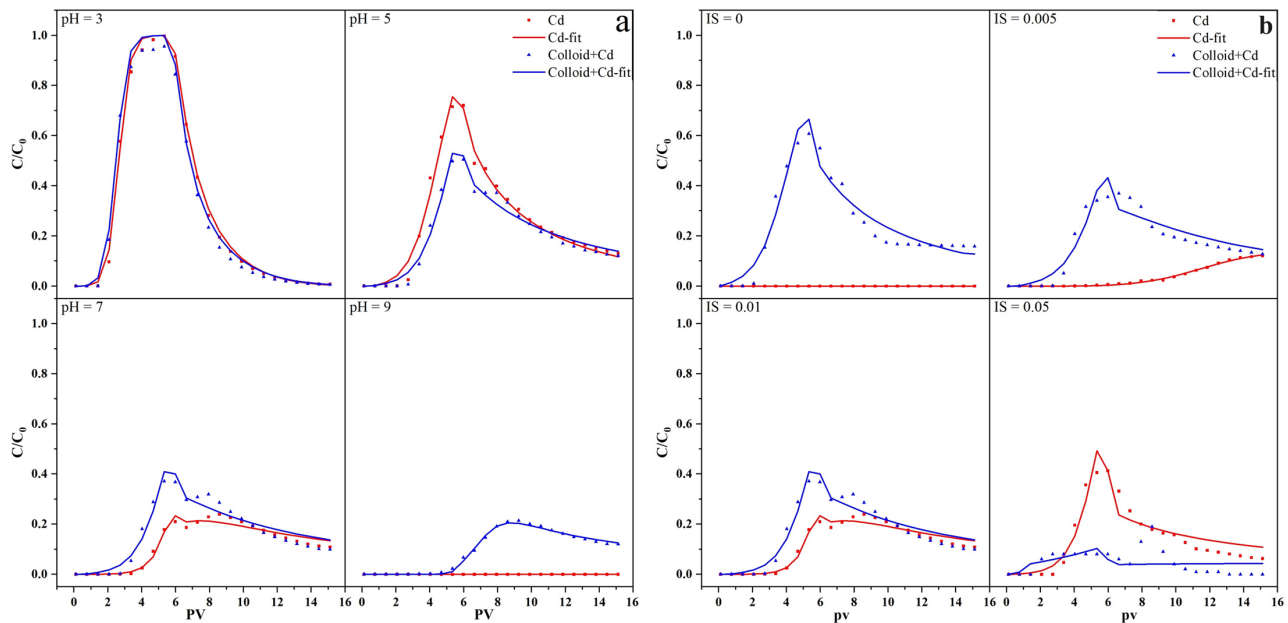


Figure 4. Cd^{2+} transport with soil colloids compare with single ion transport under different pH (a) and ionic strength (b) conditions.

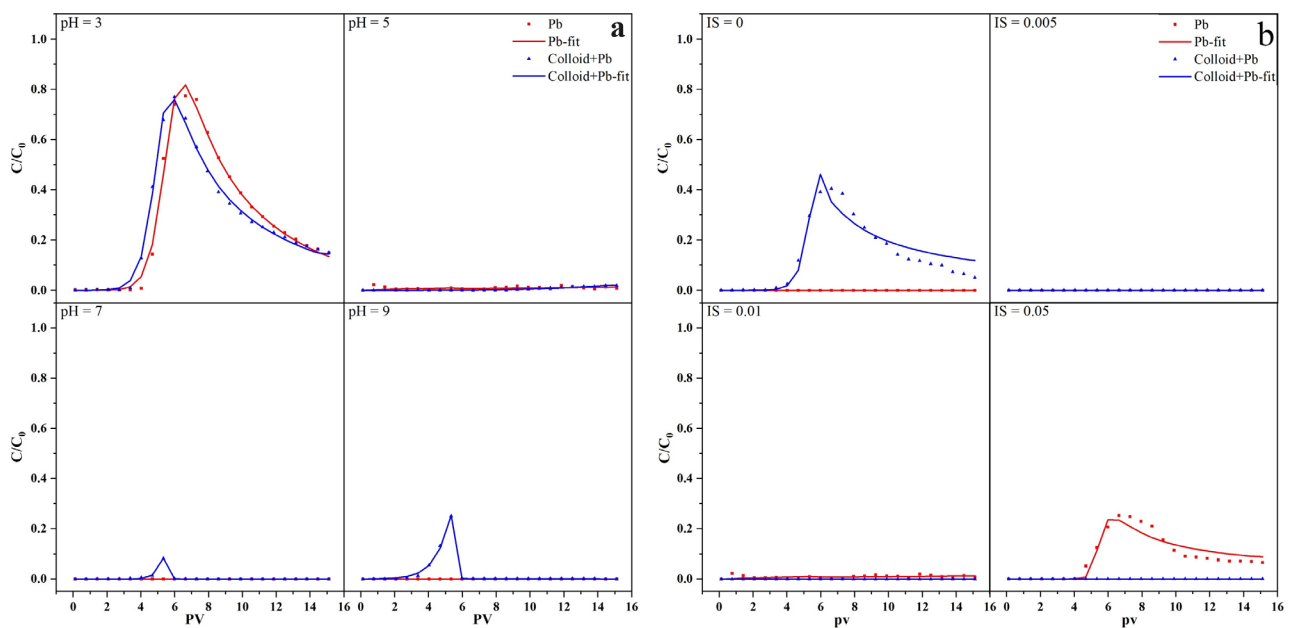


Figure 5. Pb^{2+} transport with soil colloids compared with single ion transport under different pH (a) and ionic strength (b) conditions.

Table 3. The fitting results of Cd²⁺ and Pb²⁺ co-transport with soil colloid BTCs under different pH and ionic strength conditions.

Solution	pH	IS	Dispersion	Pore	Recoveries	R ²
100 mg·L ⁻¹ Colloid + 10 mg·L ⁻¹ Cd ²⁺	3.0	0.01	0.2518	0.46	99.6%	0.9978
	5.0	0.01	0.2518	0.46	66.2%	0.9768
	7.0	0.01	0.2518	0.46	54.3%	0.9421
	9.0	0.01	0.2518	0.46	29.6%	0.9938
	7.0	0	0.2518	0.46	77.7%	0.9467
	7.0	0.005	0.2518	0.46	56.5%	0.9024
	7.0	0.05	0.2518	0.46	14.6%	0.1546
100 mg·L ⁻¹ Colloid + 10 mg·L ⁻¹ Pb ²⁺	3.0	0.01	0.2518	0.46	81.4%	0.9962
	5.0	0.01	0.2518	0.46	NA ¹	
	7.0	0.01	0.2518	0.46	1.3%	0.9920
	9.0	0.01	0.2518	0.46	6.4%	0.9968
	5.0	0	0.2518	0.46	46.2%	0.9154
	5.0	0.005	0.2518	0.46	NA ¹	
	5.0	0.05	0.2518	0.46	NA ¹	

¹ NA: not applicable.

The BTCs and Cd²⁺ recovery at pH 3.0 transport with soil colloids were similar to that of Cd²⁺ transport alone (Figure 4a), since under strongly acidic conditions, Cd²⁺ was mainly in the free state and the adsorption capacity of soil colloids and sand grains for Cd²⁺ was very low [39]. At pH 5.0, the BTC peak of Cd²⁺ with soil colloids was lower and the initial breakthrough lagged slightly. The recovery was decreased by 16.06% compared without soil colloids (Tables 2 and 3), indicating that the transport of Cd²⁺ was inhibited by soil colloids. The soil colloids were blocked in the column (Table 1) and some Cd²⁺ might be adsorbed. At pHs 7.0 and 9.0, the BTCs' peak for Cd²⁺ was higher and recoveries were increased by 15.6% and 29.6% compared without soil colloids, indicating that the transport of Cd²⁺ was facilitated by soil colloids. It was worth noting that the soil colloid recoveries were 7.0% and 32.5%, and the promotability to Cd²⁺ was not high relative to the high recoveries of colloids at pH 9.0. This occurred in a similar study [10], whereby probably was influenced by the formation of Fe/Mn (oxy)hydroxides under alkaline conditions. Fe/Mn (oxy)hydroxides enhance the non-uniformity of the surface charge on Fe/Mn-associated soil colloids, which facilitated their attachment to sand grains [11]. Remarkably at pH 7.0, the initial breakthrough of Cd²⁺ with soil colloids appeared ahead at about 1 PV while that of soil colloids appeared at about 3 PV (Figure 1a). In addition, the BTC of Cd²⁺ with soil colloids had a more gradual tailing at pH 9.0 than that of soil colloid. These phenomena indicated that soil colloids facilitated the transport of Cd²⁺ and were not only acting as carriers, but might also be an indirect effect such as the interaction changing between Cd²⁺ and sand grains or the speciation changing of Cd²⁺. At IS 0, 0.005, and 0.01 mol L⁻¹ NaNO₃, the BTCs' peak of Cd²⁺ with soil colloids was higher (Figure 4b) and recoveries were increased by 77.7%, 45.8%, and 15.6% compared without soil colloids, indicating that the transport of Cd²⁺ was facilitated by soil colloids. The BTC of Cd²⁺ with soil colloids at IS 0 and 0.01 mol L⁻¹ NaNO₃ also had a more gradual tailing and was more ahead of the initial breakthrough than soil colloids, which were similar with those at pH 7.0 and 9.0. The promotability of soil colloids to Cd²⁺ decreased with increasing ionic strength due to the soil colloid recoveries decreased from 81.6% to 7.0%. At IS 0.05 mol L⁻¹ NaNO₃, Cd²⁺ recovery was decreased by 33.1% compared without soil colloids, indicating that the transport of Cd²⁺ was inhibited by soil colloids. But an initial breakthrough of Cd²⁺ with soil colloids appeared ahead at about 1 PV while that of without soil colloids appeared at about 2 PV. The results might indicate that a few soil colloids inhibited the adsorption to Cd²⁺ by sand grains at the initial time. Then, many soil colloids were blocked in the column under high-ionic-strength conditions and inhibited the transport of Cd²⁺. In addition, the BTC of Cd²⁺ at IS 0.05 mol L⁻¹ NaNO₃ displayed a weak fitting to the model (R² = 0.1546), indicating the instability of Cd²⁺, due to the competitive adsorption of other ions.

At pH 3.0, the BTC peak of Pb^{2+} were lower (Figure 5a) and recoveries were decreased by 4.9% compared without soil colloids, indicating that the transport of Pb^{2+} was slightly inhibited by soil colloids, due to the low adsorption capacity of soil colloids for Pb^{2+} under strongly acidic condition [38,40]. At pH 5.0, soil colloids could not make an influence on the transport of Pb^{2+} ; the recovery was still 0.0% due to the soil colloids also being blocked in the column (Table 1). At pHs 7.0 and 9.0, the BTCs peak of Pb^{2+} were higher and recoveries were increased by 1.3% and 6.4% compared without soil colloids, indicating that the transport of Pb^{2+} was facilitated by soil colloids. The BTC shape of Pb^{2+} with soil colloids was similar with that of soil colloids, indicating the colloidal transport of Pb^{2+} under alkaline conditions. It is noteworthy that the recoveries of soil colloids were 7.0% and 32.5%. The promotability of soil colloids to Pb^{2+} was relatively weaker than Cd^{2+} . AF4-ICP-MS characterization found that Pb^{2+} was highly adsorbed by Fe (oxy)hydroxide (Figure 1). However, the formation of Fe (oxy)hydroxides under alkaline conditions could facilitate the attachment of Fe-associated soil colloids to sand grains [11]. At IS 0 mol L⁻¹ NaNO₃, the BTC peak of Pb^{2+} was higher (Figure 5b) and recoveries were increased by 46.2% compared without soil colloids, indicating the transport of Pb^{2+} was facilitated by soil colloids under extremely low ionic strength. At IS 0.005, 0.01 and 0.05 mol L⁻¹ NaNO₃, the Pb^{2+} recoveries with soil colloids were 0.0%, soil colloids were blocked in the column and inhibited the transport of Pb^{2+} . The transport of Pb^{2+} was mainly dependent on soil colloids except at pH 3.0.

In summary, high pH and low ionic strength were both beneficial to the transport of soil colloids, and the transport of Cd^{2+} and Pb^{2+} could be facilitated by soil colloids. However, in acidic conditions, the agglomeration retention of soil colloids within the column inhibited the transport of Cd^{2+} and Pb^{2+} , which is similar to the result of research about the arsenic (V) transport with soil colloids [15]. It has been found that the co-transport of Cd^{2+} by soil colloids is pronounced at high pH and low ionic strength and can generate a potential environmental risk [10]. Increasing pH and decreasing ionic strength of soil solution are common during irrigation, rainfall and the remediation of polluted soil. Therefore, the transport of Cd^{2+} and Pb^{2+} associated with soil colloids facilitated by increasing pH and decreasing ionic strength should be paid more attention to during these situations.

4. Conclusions

AF4-ICP-MS characterization of three contaminated natural soil solutions showed that nano-sized colloids in soil were mainly distributed in two size ranges: 0.3–35 kDa and 280 kDa–450 nm, which defined as fine nanoparticles and larger nanoparticles, mainly consisted of OM, Fe, and Mn (oxy)hydroxides and clay minerals. Cd and Pb could strongly and stably be adsorbed by fine nanoparticles under all environmental conditions. Mn and Fe (oxy)hydroxides generally formed in quantities under neutral to alkaline conditions. Cd could be adsorbed by Fe/Mn colloids and Pb was fixed by them. Column transport experiments showed that soil colloids were gradually blocked in the column with decreasing pH and increasing IS due to the reduction of negative charges on the surface and colloid agglomeration. The transport capacity of Cd^{2+} and Pb^{2+} without soil colloids gradually decreased with increasing pH and decreasing IS. The transport of Pb^{2+} without soil colloids showed stronger sensitivity to environmental conditions and was more difficult to transport than Cd^{2+} . Soil colloids inhibited the transport of Cd^{2+} and Pb^{2+} under acidic conditions due to the adsorption by the soil colloids blocked in the column. Soil colloids facilitated the transport of Cd^{2+} and Pb^{2+} under non-acidic conditions. Soil colloids facilitated the transport of Pb^{2+} which mainly act as carriers, but facilitated the transport of Cd^{2+} by carriers and indirect effect. Fe/Mn (oxy)hydroxide colloids formed in quantity under alkaline conditions but some of them might be blocked in the column, which result in the relatively weaker promotability of soil colloid. At IS 0, 0.005, and 0.01 mol L⁻¹ NaNO₃, soil colloids facilitated the transport of Cd^{2+} and the promotability decreased with the increasing IS. It was only at 0 mol L⁻¹ NaNO₃ where soil colloids facilitated the transport of Pb^{2+} . The increase in pH and decrease in ionic strength of the soil is particularly significant

during heavy irrigation and rainfall. Soil colloids will not only transport underground but also transport in large quantities with surface runoff; Cd^{2+} and Pb^{2+} will transport at the same time, which can generate a potential environmental risk.

Supplementary Materials: The following supporting information can be downloaded at: <https://www.mdpi.com/article/10.3390/agronomy14020352/s1>, Figure S1: UV full wavelength scanning signal graph of soil colloids (a: DBS, pH = 5.5; b: SY, pH = 8.0; c: HD, pH = 7.0; d: HD background, pH = 7.0); Figure S2: Relationship between soil colloid concentration and absorbance at 254 nm; Figure S3: Relationship between polystyrene sulfonate standards and elution time; Figure S4: Schematic diagram of the experimental equipment for saturated sand column; Table S1: Soil basic chemical parameters for three contaminated soils; Table S2: The Hydrus-1D fitting results of Cd^{2+} and Pb^{2+} BTCs at different pH and ionic strength conditions.

Author Contributions: Conceptualization, Z.Y. and H.X.; methodology, J.Z. and Y.Z.; software, Z.Y.; validation, Z.Y., J.Z. and W.L.; formal analysis, D.X.; investigation, S.G.; resources, D.X.; data curation, S.G.; writing—original draft preparation, Z.Y.; writing—review and editing, W.L.; visualization, Z.Y.; supervision, J.W.; project administration, Y.L. and W.L.; funding acquisition, Y.L. and W.L. All authors have read and agreed to the published version of the manuscript.

Funding: This research was funded by The National Key Research and Development Program of China (2019YFC1804400), The National Natural Science Foundation of China (41977126), and the Guangdong Basic and Applied Basic Research Foundation (2020A1515010556), The Local Innovation and Entrepreneurship Team Project of Guangdong Special Support Program (2019BT02L218), The Science and Technology Planning Project of Guangzhou (2023A04J1989), Guizhou Provincial Science and Technology Projects (QKHZC [2023] YB217), and The Open Competition Program of Ten Major Directions of Agricultural Science and Technology Innovation for the 14th Five-Year Plan of Guangdong Province (2022SDZG07, 2022SDZG08).

Data Availability Statement: Data are available under reasonable request.

Acknowledgments: We thank Jun Tang, Institute of Soil Science, Chinese Academy of Sciences, Nanjing, for help with AF4-ICP-MS measurements. We thank the Institute of Surface-Earth System Science, Tianjin University for help with soil collection.

Conflicts of Interest: The authors declare no conflicts of interest.

References

1. Bradl, H.B. Adsorption of heavy metal ions on soils and soils constituents. *J. Colloid Interface Sci.* **2004**, *277*, 1–18. [[CrossRef](#)]
2. He, S.; Lu, Q.; Li, W.; Ren, Z.; Zhou, Z.; Feng, X.; Zhang, Y.; Li, Y. Factors controlling cadmium and lead activities in different parent material-derived soils from the Pearl River Basin. *Chemosphere* **2017**, *182*, 509–516. [[CrossRef](#)]
3. Hu, B.; Shao, S.; Ni, H.; Fu, Z.; Hu, L.; Zhou, Y.; Min, X.; She, S.; Chen, S.; Huang, M.; et al. Current status, spatial features, health risks, and potential driving factors of soil heavy metal pollution in China at province level. *Environ. Pollut.* **2020**, *266*, 114961. [[CrossRef](#)]
4. de Jonge, L.W.; Kjaergaard, C.; Moldrup, P. Colloids and colloid-facilitated transport of contaminants in soils: An introduction. *Vadose Zone J.* **2004**, *3*, 321–325. [[CrossRef](#)]
5. Shaheen, S.M.; Tsadilas, C.D.; Rinklebe, J. A review of the distribution coefficients of trace elements in soils: Influence of sorption system, element characteristics, and soil colloidal properties. *Adv. Colloid Interface Sci.* **2013**, *201*, 43–56. [[CrossRef](#)] [[PubMed](#)]
6. Xu, G.; Chen, C.; Shen, C.; Zhou, H.; Wang, X.; Cheng, T.; Shang, J. Hydrogen peroxide and high-temperature heating differently alter the stability and aggregation of black soil colloids. *Chemosphere* **2022**, *287*, 132018. [[CrossRef](#)] [[PubMed](#)]
7. Sen, T.K.; Khilar, K.C. Review on subsurface colloids and colloid-associated contaminant transport in saturated porous media. *Adv. Colloid Interface Sci.* **2006**, *119*, 71–96. [[CrossRef](#)]
8. Li, Z.; Zhou, L. Cadmium transport mediated by soil colloid and dissolved organic matter: A field study. *J. Environ. Sci.* **2010**, *22*, 106–115. [[CrossRef](#)] [[PubMed](#)]
9. Mo, X.; Siebecker, M.G.; Gou, W.; Li, L.; Li, W. A review of cadmium sorption mechanisms on soil mineral surfaces revealed from synchrotron-based X-ray absorption fine structure spectroscopy: Implications for soil remediation. *Pedosphere* **2021**, *31*, 11–27. [[CrossRef](#)]
10. Liu, G.; Xue, W.; Wang, J.; Liu, X. Transport behavior of variable charge soil particle size fractions and their influence on cadmium transport in saturated porous media. *Geoderma* **2019**, *337*, 945–955. [[CrossRef](#)]

11. Zhou, D.; Wang, D.; Cang, L.; Hao, X.; Chu, L. Transport and re-entrainment of soil colloids in saturated packed column: Effects of pH and ionic strength. *J. Soils Sediments* **2011**, *11*, 491–503. [[CrossRef](#)]
12. Crancon, P.; Pili, E.; Charlet, L. Uranium facilitated transport by water-dispersible colloids in field and soil columns. *Sci. Total Environ.* **2010**, *408*, 2118–2128. [[CrossRef](#)]
13. Won, J.; Wirth, X.; Burns, S.E. An experimental study of cotransport of heavy metals with kaolinite colloids. *J. Hazard. Mater.* **2019**, *373*, 476–482. [[CrossRef](#)]
14. Zhang, W.; Jiang, F.; Sun, W. Investigating colloid-associated transport of cadmium and lead in a clayey soil under preferential flow conditions. *Water Sci. Technol.* **2021**, *84*, 2486–2498. [[CrossRef](#)] [[PubMed](#)]
15. Ma, J.; Guo, H.; Lei, M.; Wan, X.; Zhang, H.; Feng, X.; Wei, R.; Tian, L.; Han, X. Blocking effect of colloids on arsenate adsorption during co-transport through saturated sand columns. *Environ. Pollut.* **2016**, *213*, 638–647. [[CrossRef](#)]
16. Wei, Z.; Zhu, Y.; Wang, Y.; Song, Z.; Wu, Y.; Ma, W.; Hou, Y.; Zhang, W.; Yang, Y. Influence of Soil Colloids on Ni Adsorption and Transport in the Saturated Porous Media: Effects of pH, Ionic Strength, and Humic Acid. *Appl. Sci.* **2022**, *12*, 6591. [[CrossRef](#)]
17. Wang, Z.; Zhang, Y.; Flury, M.; Zou, H. Freeze-thaw cycles lead to enhanced colloid-facilitated Pb transport in a Chernozem soil. *J. Contam. Hydrol.* **2022**, *251*, 104093. [[CrossRef](#)] [[PubMed](#)]
18. Zhang, W.; Liang, Y.; Sun, H.; Wang, X.; Zhou, Q.; Tang, X. Initial soil moisture conditions affect the responses of colloid mobilisation and associated cadmium transport in opposite directions. *J. Hazard. Mater.* **2023**, *448*, 130850. [[CrossRef](#)] [[PubMed](#)]
19. Lee, S.; Ko, I.; Yoon, I.; Kim, D.; Kim, K. Colloid mobilization and heavy metal transport in the sampling of soil solution from Duckum soil in South Korea. *Environ. Geochem. Health* **2019**, *41*, 469–480. [[CrossRef](#)] [[PubMed](#)]
20. Hu, P.; Zhang, Y.; Wang, J.; Du, Y.; Wang, Z.; Guo, Q.; Pan, Z.; Ma, X.; Planer-Friedrich, B.; Luo, Y.; et al. Mobilization of Colloid- and Nanoparticle-Bound Arsenic in Contaminated Paddy Soils during Reduction and Reoxidation. *Environ. Sci. Technol.* **2023**, *57*, 9843–9853. [[CrossRef](#)] [[PubMed](#)]
21. Vega, F.A.; Weng, L. Speciation of heavy metals in River Rhine. *Water Res.* **2013**, *47*, 363–372. [[CrossRef](#)] [[PubMed](#)]
22. Bergen, B.; Moens, C.; De Winter, A.; Ricou, F.; Smolders, E. Colloids facilitate cadmium and uranium transport in an undisturbed soil: A comparison of soil solution isolation methods. *Sci. Total Environ.* **2023**, *890*, 164419. [[CrossRef](#)] [[PubMed](#)]
23. Du, L.; Cuss, C.W.; Dyck, M.F.; Noernberg, T.; Shoty, W. Size-resolved analysis of trace elements in the dissolved fraction (<0.45 µm) of soil solutions using a novel lysimeter and asymmetrical flow field-flow fractionation coupled to ultraviolet absorbance and inductively coupled plasma mass spectrometry. *Can. J. Soil Sci.* **2020**, *100*, 381–392. [[CrossRef](#)]
24. Regelink, I.C.; Weng, L.; Koopmans, G.F.; van Riemsdijk, W.H. Asymmetric flow field-flow fractionation as a new approach to analyse iron-(hydr)oxide nanoparticles in soil extracts. *Geoderma* **2013**, *202–203*, 134–141. [[CrossRef](#)]
25. Chotpantarat, S.; Kiatvarangkul, N. Facilitated transport of cadmium with montmorillonite KSF colloids under different pH conditions in water-saturated sand columns: Experiment and transport modeling. *Water Res.* **2018**, *146*, 216–231. [[CrossRef](#)]
26. Wikiniyadhane, R.; Chotpantarat, S.; Ong, S.K. Effects of kaolinite colloids on Cd²⁺ transport through saturated sand under varying ionic strength conditions: Column experiments and modeling approaches. *J. Contam. Hydrol.* **2015**, *182*, 146–156. [[CrossRef](#)]
27. Jiang, Z.; Nie, K.; Arinzechi, C.; Li, J.; Liao, Q.; Si, M.; Yang, Z.; Li, Q.; Yang, W. Cooperative effect of slow-release ferrous and phosphate for simultaneous stabilization of As, Cd and Pb in soil. *J. Hazard. Mater.* **2023**, *452*, 131232. [[CrossRef](#)]
28. Neubauer, E.; Kammer, F.V.D.; Hofmann, T. Using FLOWFFF and HPSEC to determine trace metal colloid associations in wetland runoff. *Water Res.* **2013**, *47*, 2757–2769. [[CrossRef](#)]
29. Regelink, I.C.; Voegelin, A.; Weng, L.; Koopmans, G.F.; Comans, R.N.J. Characterization of Colloidal Fe from Soils Using Field-Flow Fractionation and Fe K-Edge X-ray Absorption Spectroscopy. *Environ. Sci. Technol.* **2014**, *48*, 4307–4316. [[CrossRef](#)]
30. Li, X.; Cao, Z.; Du, Y.; Zhang, Y.; Wang, J.; Ma, X.; Hu, P.; Luo, Y.; Wu, L. Multi-metal contaminant mobilizations by natural colloids and nanoparticles in paddy soils during reduction and reoxidation. *J. Hazard. Mater.* **2024**, *461*, 132684. [[CrossRef](#)] [[PubMed](#)]
31. Hu, J.; Zevi, Y.; Kou, X.; Xiao, J.; Wang, X.; Jin, Y. Effect of dissolved organic matter on the stability of magnetite nanoparticles under different pH and ionic strength conditions. *Sci. Total Environ.* **2010**, *408*, 3477–3489. [[CrossRef](#)]
32. Kubier, A.; Wilkin, R.T.; Pichler, T. Cadmium in soils and groundwater: A review. *Appl. Geochem.* **2019**, *108*, 104388. [[CrossRef](#)]
33. Wang, Y.; Fruttschi, M.; Suvorova, E.; Phrommavanh, V.; Descostes, M.; Osman, A.A.A.; Geipel, G.; Bernier-Latmani, R. Mobile uranium (IV)-bearing colloids in a mining-impacted wetland. *Nat. Commun.* **2013**, *4*, 2942. [[CrossRef](#)] [[PubMed](#)]
34. Wang, D.; Jiang, X.; Rao, W.; He, J. Kinetics of soil cadmium desorption under simulated acid rain. *Ecol. Complex.* **2009**, *6*, 432–437. [[CrossRef](#)]
35. Liu, F.; Xu, B.; He, Y.; Brookes, P.C.; Tang, C.; Xu, J. Differences in transport behavior of natural soil colloids of contrasting sizes from nanometer to micron and the environmental implications. *Sci. Total Environ.* **2018**, *634*, 802–810. [[CrossRef](#)] [[PubMed](#)]
36. Bradford, S.A.; Morales, V.L.; Zhang, W.; Harvey, R.W.; Packman, A.I.; Mohanram, A.; Welty, C. Transport and Fate of Microbial Pathogens in Agricultural Settings. *Crit. Rev. Environ. Sci. Technol.* **2013**, *43*, 775–893. [[CrossRef](#)]
37. Bradford, S.A.; Torkzaban, S.; Walker, S.L. Coupling of physical and chemical mechanisms of colloid straining in saturated porous media. *Water Res.* **2007**, *41*, 3012–3024. [[CrossRef](#)] [[PubMed](#)]

38. Won, J.; Burns, S.E. Role of Immobile Kaolinite Colloids in the Transport of Heavy Metals. *Environ. Sci. Technol.* **2018**, *52*, 2735–2741. [[CrossRef](#)] [[PubMed](#)]
39. Liu, G.; Wang, J.; Xue, W.; Zhao, J.; Wang, J.; Liu, X. Effect of the size of variable charge soil particles on cadmium accumulation and adsorption. *J. Soils Sediments* **2017**, *17*, 2810–2821. [[CrossRef](#)]
40. Egwu, G.N.; Agbenin, J.O. Lead enrichment, adsorption and speciation in urban garden soils under long-term wastewater irrigation in northern Nigeria. *Environ. Earth Sci.* **2013**, *69*, 1861–1870. [[CrossRef](#)]

Disclaimer/Publisher’s Note: The statements, opinions and data contained in all publications are solely those of the individual author(s) and contributor(s) and not of MDPI and/or the editor(s). MDPI and/or the editor(s) disclaim responsibility for any injury to people or property resulting from any ideas, methods, instructions or products referred to in the content.